Draft version February 2, 2008
Preprint typeset using LaTeX style emulateapj v. 11/12/01

SEARCHES FOR FAST RADIO TRANSIENTS

J. M. Cordes[1] & M. A. McLaughlin[2]
Draft version February 2, 2008

ABSTRACT

We discuss optimal detection of fast radio transients from astrophysical objects while taking into account the effects of propagation through intervening ionized media, including dispersion, scattering and scintillation. Our analysis applies to the giant-pulse phenomenon exhibited by some pulsars, for which we show examples, and to radio pulses from other astrophysical sources, such as prompt radio emission from gamma-ray burst sources and modulated signals from extra-terrestrial civilizations. We estimate scintillation parameters for extragalactic sources that take into account scattering in both the host galaxy and in foreground, Galactic plasma.

Subject headings: radio pulses, pulsars, interstellar medium, dispersion, scattering, gamma-ray bursts, SETI

1. INTRODUCTION

Fast radio transients – pulses with durations of seconds or less – are important indicators of coherent emission processes in astrophysical sources. The detection of such pulses is complicated by their propagation through the intervening ionized media. We focus on the interstellar medium (ISM) in this paper, but the intergalactic and interplanetary media are also relevant for some objects. The dominant effects, dispersion and scattering, distort pulses but also provide a signature for distinguishing them from terrestrial radio-frequency interference (RFI). In this paper we discuss algorithms for detecting pulses that are dispersed and scattered to varying degrees by the ISM. This discussion is quite general. Though it is motivated by pulsar radio emission, particularly the so-called 'giant-pulses' from the Crab pulsar and a few other objects, our analysis applies to any other transient radio source.

Searches for radio transients have a long history. Indeed, pulsars were first discovered by the detection of single pulses on a chart recorder (Hewish et al. 1968), with the Crab pulsar detected through its giant pulses soon after (Staelin & Reifenstein 1968). Davies & Large (1970) detected three new pulsars in their single-pulse search but failed to detect any pulses from 13 supernova remnants. A search for single pulses from the X-ray sources Scorpius X-1 and Cygnus X-1, at one time thought to be possibly associated with pulsars, was also unsuccessful (Taylor et al. 1972). In a search for radio counterparts to the gravitational pulses reported by Weber (1969), both Hughes & Retallack (1973) and Edwards et al. (1974) detected excesses of radio pulses from the direction of the Galactic center, but did not believe them to be correlated with the gravitational pulses. With the goal of detecting the single, large radio pulse expected to be emitted at the time of a supernova explosion (Colgate & Noerdlinger 1971), Huguenin & Moore (1974) and Kardashev et al. (1977) performed radio searches for single pulses, but found no convincing signals of extraterrestrial origin aside from solar flares. O'Sullivan et al. (1978) and Phinney & Taylor (1979) conducted searches for radio bursts possibly associated with annihilating black holes, as suggested by Rees (1977), but likewise found no convincing signals. Linscott & Erkes (1980) reported the detection of highly dispersed pulses from the elliptical galaxy M87, at a distance of roughly 15 Mpc, attributing these pulses to a massive compact object at the center. However, subsequent attempts by others to confirm their findings were unsuccessful (Hankins et al. 1981; McCulloch et al. 1981; Taylor et al. 1981). In searches for radio pulses associated with gamma-ray bursts, Cortiglioni et al. (1981), Inzani et al. (1982) and Amy et al. (1989) detected some dispersed radio pulses, but found no convincing associations with gamma-ray burst sources. Vaughan & Large (1989) also conducted an unsuccessful search for radio pulses from the soft gamma-ray repeater 0526−66. More recently, Nice (1999) searched for radio pulses along 68 deg^2 of the Galactic plane at 430 MHz. This search resulted in the detection of individual pulses from 5 known pulsars and the discovery of one new pulsar which was previously missed in a standard periodicity search (Nice et al. 1995). This pulsar (J1918+08) does not emit giant pulses[3] but is a normal, slow pulsar which fortuitously emitted one strong pulse during the search observations.

The modest success of these searches for transient radio signals has been largely due to limited sensitivity and sky coverage and, most importantly, to the difficulty in discriminating between signals of astrophysical origin and RFI. Array instruments such as the Low Frequency Array (LOFAR) and the Square Kilometer Array (SKA) will be a vast improvement over single-dish systems in all of these areas. With these arrays in the developmental stages, it is timely to revisit searches for single pulses. The outline of this paper is as follows. In §2, we discuss the objects that might be sources of transient radio signals. In §3, we describe single-pulse search algorithms and present example results for giant-pulse emitting pulsars. We

[1] Astronomy Department and NAIC, Cornell University, Ithaca, NY 14853
[2] Jodrell Bank Observatory, University of Manchester, Macclesfield, Cheshire, SK11 9DL, UK
[3] We define giant pulses as those comprising a long tail on the overall pulse amplitude distribution; for the Crab pulsar and the millisecond pulsars B1937+21 and B1821-24, these distributions are power-law in form.

discuss dispersion and pulse broadening from scattering, their effects on searches for single pulses, and ways to optimize searches in the presence of these effects. In §4, the effects of scintillations on source detection are outlined. As the increasing prominence of RFI makes it difficult to identify transient pulses, we briefly discuss RFI issues in §5. Conclusions and a look to the future, especially for RFI mitigation, are offered in §6. In Paper II (McLaughlin & Cordes 2003), we explicitly discuss giant pulses from Galactic pulsars and our attempts to detect similar pulses from nearby galaxies. In that paper we also outline the conditions required for single-pulse searches to be more effective than periodicity searches for pulsars.

2. SOURCES OF FAST RADIO TRANSIENTS

While all pulsars show pulse-to-pulse intensity variations (Hesse & Wielebinski 1974), some pulsars have been found to emit so-called 'giant' pulses, pulses with strengths 100 or even 1000 times the mean pulse intensity. The Crab (PSR B0531+21) was the first pulsar found to exhibit this phenomenon. In one hour of observation, the largest measured peak pulse flux of the Crab is roughly $\sim 10^5$ Jy at 430 MHz for a duration of roughly 100 μs (Hankins & Rickett 1975), corresponding to an implied brightness temperature of 10^{31} K. Recently, pulses with flux $\sim 10^3$ Jy at 5 GHz for a duration of only 2 ns have been detected from the Crab (Hankins 2003). These 'nano-giant' pulses imply brightness temperatures of 10^{38} K, by far the most luminous emission from any astronomical object. For many years, this phenomenon was thought to be uniquely characteristic of the Crab. However, giant pulses have since been detected from the millisecond pulsars PSR B1937+21 and PSR B1821−24. From both of these pulsars, the largest measured peak pulse flux in one hour is $\sim 10^3$ Jy at 430 MHz (Cognard et al. 1996; Romani & Johnston 2001). Recently, giant pulses have been detected from the Crab-like pulsar in the Large Magellanic Cloud, PSR B0540-69 (Johnston & Romani, 2003).

Although pulsars may be the most well-studied transient radio sources, they are by no means the only ones. In Figure 1, we compare the brightness temperatures of giant pulses with those from other astrophysical sources of radio pulses. These sources include brown dwarfs such as BD LP944−20, from which radio flares have recently been detected (Berger et al. 2001), and Jupiter, which has long been known to emit radio flares at decameter wavelengths (Aubier et al. 2000; Lecacheux et al. 1998). Type II and Type III solar bursts are regularly detected at radio frequencies of tens of MHz (Mann et al. 1996; Poquerusse et al. 1988). Radio flares from active stars such as UV Ceti and AD Leo are observed at frequencies $\sim$ 1 GHz (Jackson et al. 1989). The emission from OH masers can vary on timescales of hundreds of seconds and be detected as long-duration radio bursts (Cohen & Brebner 1985; Yudaeva 1986). Active galactic nuclei (AGN) outbursts, likely due to propagation of shocks in relativistic jets, are observed at millimeter and centimeter wavelengths (Aller et al. 1985; Lainela 1994). Intraday variability (IDV) of other extragalactic sources, most likely caused by interstellar scintillation, could also be detectable in searches for radio transients (Kedziora-Chudczer et al. 2001). Gamma-ray burst (GRB) afterglows are also modulated by refractive, and possibly diffractive, scintillation (Goodman 1997). Radio bursts from supernovae, as proposed by Colgate (1971) and detected from supernova 1987a (Turtle et al. 1987), bursts from the explosions of primordial black holes (Phinney & Taylor 1979), and emission from inspiraling neutron stars (Hansen & Lyutikov 2000) could also be sources of fast radio transients. Finally, searches for radio transients could detect scintillation-modulated signals from extraterrestrial intelligent civilizations (Cordes et al. 1997).

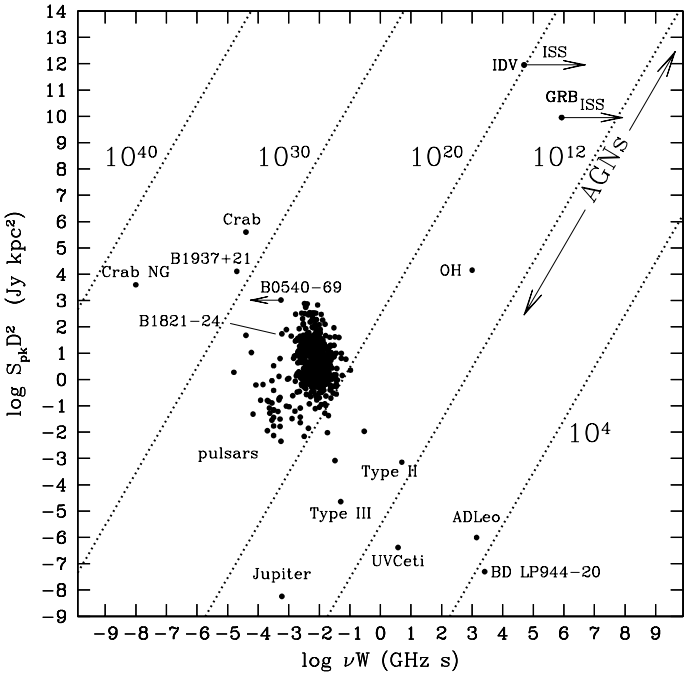

FIG. 1.— A log-log plot of the product of peak flux S in Jy and the square of the distance D in kpc vs. the product of frequency ν in GHz and pulse width W in s. Points are shown for the 'nano-giant' pulses detected from the Crab (Hankins et al. 2003), the giant pulses detected from the Crab, PSR B1937+21 and PSR B1821−24, single pulses from all pulsars with flux, distance and pulse width listed in the Princeton Pulsar Catalog (Taylor et. al 1993) and other possible sources of radio bursts. Lines of constant brightness temperature $T = SD^2/2k(\nu W)^2$ are shown, where k is Boltzmann's constant. See text for explanations of particular plotted symbols.

3. SINGLE-PULSE SEARCH METHODOLOGY

In this section, we describe general issues that must be considered in designing and carrying out any search for transient radio signals. We first explore the various factors influencing the intensities, shapes and widths of detected radio pulses. We then outline the steps of a search for dispersed radio pulses, including dedispersion, matched filtering, thresholding and diagnostics to determine the reality of detected signals. Lastly, we describe the effects that interstellar scattering and scintillation have on searches for fast radio transients and how to optimize searches in the presence of these effects.

3.1. *Signal Model*

An appropriate model[4] for the measured intensity from a broadband source is

$$I(t) = g_{\rm r} g_{\rm d} S(t) * h_{\rm DM}(t) * h_{\rm d}(t) * h_{\rm Rx}(t) + N(t), \quad (1)$$

where the source contribution, $S(t)$, is modulated by factors $g_{\rm r}$ and $g_{\rm d}$ that correspond to refractive and diffractive scintillation modulations (see below) while also being convolved (denoted by the asterisks) with several factors that account for dispersion smearing, $h_{\rm DM}(t)$, pulse-broadening from multipath propagation, $h_{\rm d}(t)$, and averaging in the receiver and data acquisition system, $h_{\rm Rx}(t)$. Additive receiver noise is represented by $N(t)$. To a large extent, dispersion smearing associated with $h_{\rm DM}(t)$ can be deconvolved from the signal. However, there can be residual dedispersion smearing if the exact value of dispersion measure (DM) is not used, as we discuss below. For large path lengths through the Galaxy and observations at low frequencies, pulse broadening from scattering can dominate the shape of the measured pulse, in which case optimal detection entails usage of an asymmetric matched filter given by the appropriate pulse broadening function, $h_{\rm d}(t)$. Below, we discuss the detection of broadband pulses with respect to these various factors.

For narrowband signals, such as those that are hypothesized from extraterrestrial civilizations, the signal model in Eq. 1 is applicable, though $S(t)$ now must be viewed as a time modulation that also depends on radio frequency. The interplay of propagation effects with the intrinsic properties of the signal need to be considered for particular cases. In this paper we address broadband pulses explicitly and simply state that many of our conclusions will also apply to modulated, narrowband signals. The effects of scintillations in particular are discussed in Cordes & Lazio (1991) and Cordes, Lazio & Sagan (1997).

3.2. *Effective Time Resolution*

The shape of a detected radio pulse is influenced by a variety of factors. A delta-function pulse emitted at the source will be detected with finite width due to a combination of propagation effects and signal-processing response times. The effective time resolution for a pulse is approximately the quadratic sum of the dispersion smearing, the dedispersion error, the receiver filter response time and scattering smearing, so that

$$\Delta t = \left[\Delta t_{\rm DM}^2 + \Delta t_{\delta\rm DM}^2 + \Delta t_{\Delta\nu}^2 + \tau_d^2\right]^{1/2}. \quad (2)$$

The first term, the frequency-dependent smearing due to dispersion, is equal to

$$\Delta t_{\rm DM} = 8.3\,\mu{\rm s}\,{\rm DM}\,\Delta\nu_{\rm MHz}\nu_{\rm GHz}^{-3} \quad (3)$$

for a bandwidth $\Delta\nu_{\rm MHz}$, an observing frequency $\nu_{\rm GHz}$ and a dispersion measure DM, where DM is defined as the column density along the line of sight (LOS) to a source (i.e. ${\rm DM} = \int_0^{\rm D} n_e(l){\rm d}l$, where n_e is the electron density and D is the distance to the source) and has units of pc cm^{-3}. Optimal detection requires that dispersion smearing be removed from the measured signal by compensating time delays or, equivalently, unwrapping phases of the Fourier components. For any such 'dedispersion' technique, using a value for DM that is in error by an amount δDM yields smearing of

$$\Delta t_{\delta\rm DM} = \Delta t_{\rm DM}(\delta{\rm DM}/{\rm DM}). \quad (4)$$

The third term, the filter response of an individual frequency channel, is

$$\Delta t_{\Delta\nu} \sim (\Delta\nu)^{-1} = (\Delta\nu_{\rm MHz})^{-1}\mu{\rm s}. \quad (5)$$

Finally, the fourth term, τ_d, is the broadening due to multipath scattering, which has the effect of convolving the intrinsic pulse profile with a function approximately exponential in form and having a characteristic time scale τ_d. Though it is highly dependent on direction and distance, it may be estimated approximately as a statistical function of DM. The mean of this dependence is given by the empirical fit (Cordes & Lazio 2002)

$$\log\tau_d = -3.72 + 0.411\log{\rm DM} + 0.937(\log{\rm DM})^2 - 4.4\log\nu_{\rm GHz}\,\mu s, \quad (6)$$

with scatter about the mean fit of $\sigma_{\log\tau_d} \approx 0.65$. The coefficient 4.4 in the last term is based on the assumption of a Kolmogorov spectrum for the scattering irregularities. For some lines of sight the scaling with frequency may be weaker (e.g. Löhmer et al. 2001), implying a coefficient closer to 4.0. In Figure 2 we illustrate some typical ISS parameters for pulsars. We further discuss pulse broadening along with interstellar scintillation modulations in §4, §4.3 and in the Appendix.

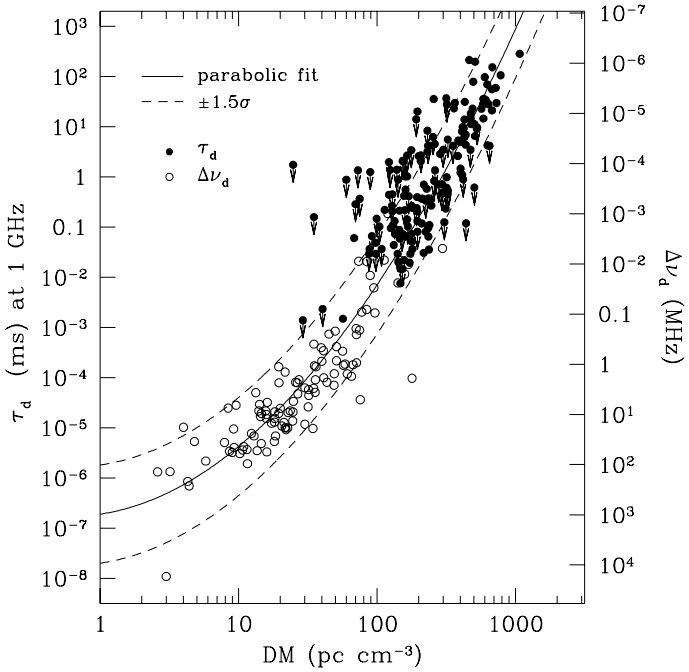

FIG. 2.— Pulse broadening time τ_d and scintillation bandwidth $\Delta\nu_{\rm d}$ plotted against DM (see Cordes & Lazio 2002 for references). The open circles represent measurements of τ_d while filled circles designate measurements of $\Delta\nu_{\rm d}$. Arrows indicate upper limits. The two quantities are related by $2\pi\tau_d\Delta\nu_{\rm d} = C_1$ with $C_1 = 1.16$ (see §4.3 for further details). All measurements have been scaled to 1 GHz from the original frequencies assuming $\tau_d \propto \nu^{-4.4}$. The solid curve is a least squares fit and the dashed lines represent $\pm1.5\sigma$ deviations from the fit.

[4] This model is only approximate. Receiver noise is strictly additive only in the limit of large signal-to-noise ratio and large time-bandwidth product. Also, the diffractive modulation $g_{\rm d}$ can be factored as shown only if it is constant over the measurement bandwidth. One may consider channelized signals for which this is true, in which case the total intensity will be the sum over channels of intensities like those given in the model. We also point out that when the diffractive scintillation modulation $g_{\rm d}$ is important (i.e. not quenched by bandwidth smoothing) multipath-induced pulse smearing is likely to be negligible and vice versa.

3.3. *Dedispersion*

While the effects of scattering cannot be removed with hardware or software, the effects of interstellar dispersion can be largely or completely corrected for. The degree to which this can be done depends on the method of dedispersion used. We discuss two methods of dedispersion and compare the time resolutions achievable with each.

3.3.1. *Post-Detection Dedispersion*

Post-detection dedispersion operates on 'detected' signals, or signals which are intensity-like quantities because a squaring operation has taken place after the signal has been channelized in a spectrometer. Typically, these data are acquired using an analog or digital multi-channel spectrometer, or 'filterbank', in which the bandpass is divided into a number of frequency channels and recorded at short time intervals after detection. Post-detection dedispersion involves shifting the signal from each frequency channel by the predicted dispersive delay for a particular DM. This delay,

$$t_{\rm DM} = 4.2 \times 10^3 \,{\rm DM}\, \nu_{\rm GHz}^{-2}\, \mu s, \tag{7}$$

is consistent with the differential form of Eq. 3.

The degree to which dispersion can be removed (i.e. the minimum time resolution for this method of dedispersion) is determined by the competing effects of $\Delta t_{\rm DM}$ and $\Delta t_{\Delta\nu}$, both of which depend on the channel bandwidth. The optimal channel bandwidth corresponds to equality of the terms $\Delta t_{\rm DM}$ and $\Delta t_{\Delta\nu}$ and is therefore $\Delta\nu_{\rm MHz} = \left(\nu_{\rm GHz}^3/8.3{\rm DM}\right)^{1/2}$. Assuming DM is known exactly (i.e. $\delta{\rm DM} = 0$), the minimum time resolution achievable through this method of dedispersion becomes

$$\Delta t_0 = \left[2(\Delta t_{\rm DM\,min})^2 + \tau_d^2\right]^{1/2} \tag{8}$$

where

$$\Delta t_{\rm DM\,min} \approx \left(8.3{\rm DM}\nu_{\rm GHz}^{-3}\right)^{1/2}\, \mu s \tag{9}$$

is the minimum dispersion smearing.

3.3.2. *Coherent Dedispersion*

Coherent, or pre-detection, dedispersion, operates on signals proportional to the electric field selected by the receiver system, which contains phase information. These data are typically acquired by bandpass filtering signal voltages and shifting them to zero frequency (i.e. 'baseband mixing'). Baseband signals are sampled according to the Nyquist criterion applied to the total bandwidth. Coherent dedispersion is being used more commonly as recording bandwidths and computer power have grown. It involves removal of the dispersive phase rotation of the (complex) electric field through a deconvolution procedure. The function to be deconvolved is approximately in the form of a 'chirp' function having duration equal to the dispersion time across the total bandwidth, given by Eq. 3. This is often done using Fourier transforms (as pioneered by Hankins in 1971) and has also been implemented using finite-impulse response, time-domain filtering (e.g. Backer et al. 1997). If the source's DM is known exactly, then the phase perturbation can be removed exactly and $\Delta t_{\rm DM} = 0$. The minimum time resolution achievable is then simply

$$\Delta t_0 = \left[\Delta t_{\Delta\nu}^2 + \tau_d^2\right]^{1/2}. \tag{10}$$

3.3.3. *Trial Dispersion Measures*

In practice, the DM is not usually known in searches for radio transients. Therefore, for either method of dedispersion, a range of trial DMs must be used to dedisperse the data. The maximum DM searched can be estimated by using a model for the Galactic electron density in the direction of the source (e.g. Cordes & Lazio 2002). Because there are significant model uncertainties owing to unmodeled electron density structures in the ISM, it is wise to search to DM values higher than predicted by the model. The spacing of trial DMs is determined by the maximum smearing one is willing to accept in the final dedispersed time series. This residual dispersion smearing is given by $\Delta t_{\delta{\rm DM}}$, calculated using Eq. 3-4 with $\Delta\nu_{\rm MHz}$ as the total bandwidth. The spacing of DM values can be calculated by letting the error from $\Delta t_{\delta{\rm DM}}$ be a fraction ϵ of the total error calculated from Eq. 2. Given that $\Delta t_{\delta{\rm DM}} = (\delta{\rm DM}/{\rm DM})\Delta t_{\rm DM}$ the required spacing of DM values in the grid is

$$\delta{\rm DM}/{\rm DM} = \frac{\epsilon \Delta t}{\Delta t_{\rm DM}} \tag{11}$$

where, for optimal resolution, $\Delta t \rightarrow \Delta t_0$. Note that as the DM increases, both $\Delta t_{\rm DM}$ and τ_d increase, making the optimal spacing between trial DMs greater at higher DMs.

We explore the effect that an incorrect DM has on an individual pulse's amplitude. For a rectangular bandpass function and for a Gaussian-shaped pulse with width W (FWHM) in milliseconds, the ratio of measured peak flux $S(\delta{\rm DM})$ to true peak flux S for a DM error $\delta{\rm DM}$ is

$$\frac{S(\delta{\rm DM})}{S} = \frac{\sqrt{\pi}}{2}\zeta^{-1}{\rm erf}\,\zeta \tag{12}$$

where

$$\zeta = 6.91 \times 10^{-3}\delta{\rm DM}\,\frac{\Delta\nu_{\rm MHz}}{W_{\rm ms}\nu_{\rm GHz}^3}. \tag{13}$$

Figures 3 and 4 illustrate the dependence of $S(\delta{\rm DM})/S$ on these quantities. Figure 3 implies a FWHM for $S(\delta{\rm DM})/S$ vs ζ, $\Delta\zeta \approx 3.5$, which corresponds to an equivalent range in DM,

$$\Delta{\rm DM} \approx 506\frac{W_{\rm ms}\nu_{\rm GHz}^3}{\Delta\nu_{\rm MHz}}. \tag{14}$$

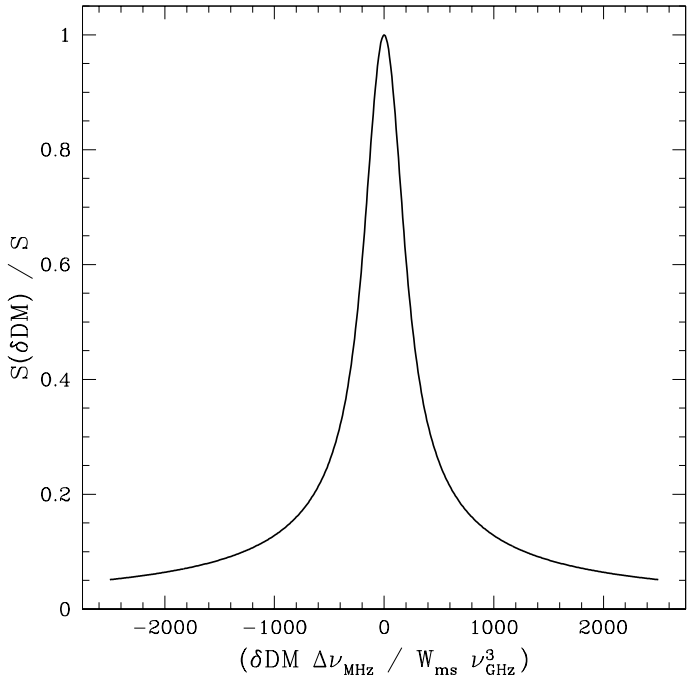

FIG. 3.— The ratio of measured peak flux to true peak flux as a function of δDM, W, $\nu_{\rm GHz}$ and $\Delta\nu_{\rm MHz}$ for δDM in pc cm^{-3} and W in ms. The abcissa is a combined factor signifying that the signal-to-noise degrades for larger errors in DM, smaller pulse widths, lower frequencies and larger bandwidths.

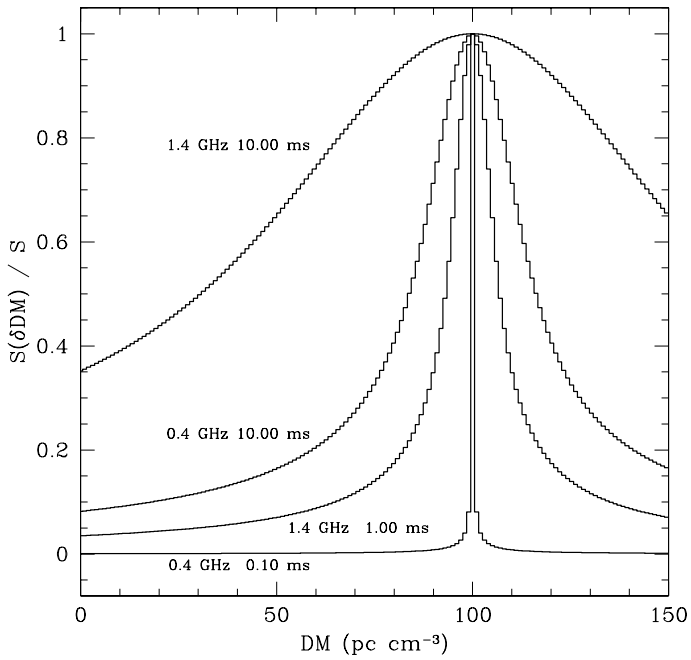

FIG. 4.— The ratio of measured flux to true flux as a function of trial DM used for dedispersion for a pulse with true DM of 100 pc cm^{-3}. Curves are labeled with observing frequency and intrinsic pulse width. Bandwidths of 10 and 100 MHz are assumed at 0.4 and 1.4 GHz, respectively.

3.4. *Matched Filtering*

After dedispersion, each dedispersed time series, or 'DM channel', must be searched individually for pulses with amplitudes above some signal-to-noise (S/N) threshold. This search process is simply an exercise in matched filtering, with the highest detected S/N achieved when the effective sampling time of the time series is equal to the detected width of the pulse. Since the intrinsic widths of signals are typically unknown, as are the contributions to the width from dispersion and scattering, a large parameter space must be searched. This is most easily done by 'smoothing' time series by adding adjacent samples iteratively. In the absence of knowledge about the true pulse shape and width, the smoothing approach is a straight-forward and efficient approximation to optimal detection.

To explore the S/Ns achievable through optimal matched filtering, first consider a pulse whose intrinsic amplitude and width are S_i and W_i, respectively, in the absence of extrinsic broadening effects. The intrinsic pulse area $A_i \approx S_i W_i$. Optimal detection implies a signal to noise ratio

$$(S/N)_i = \frac{1}{\sigma\sqrt{W_n}}\left(\frac{A_i}{\sqrt{W_i}}\right), \qquad (15)$$

where σ is the rms noise in the time series (before any smoothing) and W_n is the correlation time for the noise. We assume that $W_i \gg W_n$. For the system noise $S_{\rm sys}$ expressed as a flux density in Jansky units, the rms radiometer noise is $\sigma = S_{\rm sys}/(N_{\rm pol}\Delta\nu W_n)^{1/2}$, where $N_{\rm pol}$ is the number of polarizations summed and $\Delta\nu$ is the total bandwidth, so that S/N in the case of optimal detection is independent of W_n. As can be seen, $S/N \propto A_i/\sqrt{W_i}$ so, for fixed pulse area, a narrower pulse yields larger S/N. However, a low-amplitude, broad pulse is more easily detectable than a sharp narrow pulse if its area is sufficiently larger.

Now consider pulses that are broadened extrinsically by the interstellar and instrumental effects discussed earlier and/or by pulse smearing from orbital motion. All of these broadening effects conserve pulse area. For heavily scattered pulses, the measured shape will be dominated by the pulse broadening function, which is approximately a one-sided exponential in form. The detailed shape is a function of the wavenumber spectrum and spatial distribution of the scattering medium (Williamson 1972; Lambert & Rickett 1999). For such cases, the appropriate matched filter would be the shape of the pulse broadening function. Pulse smearing from orbital motion is negligible for known radio pulsar binaries (i.e. orbital periods $\geq$ 1 hr) and for intrinsic pulse durations of seconds or less. However, for very short-period binaries, such as two neutron stars undergoing inspiral from gravitational radiation, and for very long-duration pulses, orbital motion may be important in single pulse detection. If such broadening results in a net pulse width W_b, then matched filtering yields

$$(S/N)_b = (S/N)_i\left(\frac{W_i}{W_b}\right)^{1/2}. \qquad (16)$$

3.5. *Thresholding*

To determine a reasonable threshold for a search for single pulses, we assume that the statistics are Gaussian in the absence of any signal, either celestial or RFI (a good assumption when the time-bandwidth product $\gtrsim 5$). The expected number of candidate pulses above threshold from radiometer noise alone in a single DM channel in a time

series of length N is

$$N(> \text{threshold}) = NP_t \sum_{j=0}^{j_{\max}} 2^{-j} \approx 2NP_t, \qquad (17)$$

where P_t is the integrated Gaussian probability of measuring a pulse above threshold, and j_{max} is the number of times a time series is smoothed and decimated. The approximate equality holds for $j_{\max} \gg 1$. The threshold can be chosen based on how many 'false alarms' (i.e. threshold crossings caused solely by radiometer noise) one is willing to accept. In reality, however, the measured statistics are not Gaussian due to the presence of RFI and the level of RFI often determines the threshold used.

Once pulses above threshold are recorded, the mean and rms can be recalculated with these 'first-pass' strongest pulses removed and the search for pulses above threshold is repeated. This iterative procedure keeps the mean and rms from being biased by a few very strong pulses. To allow for any long-term level changes, small ($\sim$ seconds) subsets of the original data set should be searched individually.

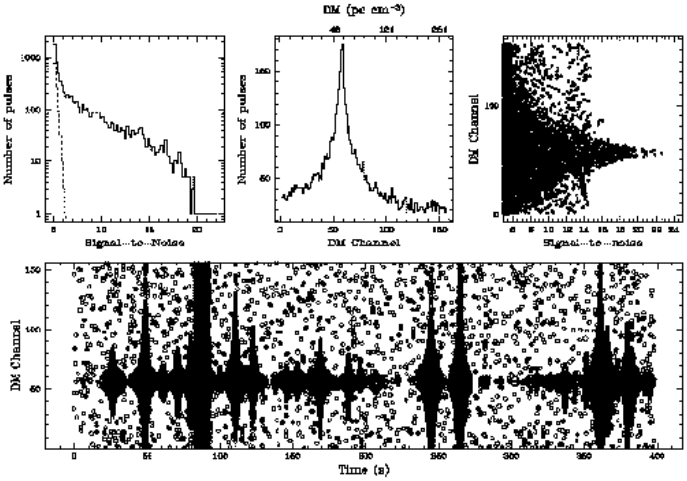

FIG. 5.— Single-pulse search results at 2330 MHz for the Crab pulsar, whose DM is 56.8 pc cm^{-3}. The pulsar's period-averaged flux density $\sim$ 3 mJy at this frequency. As described in the text, each time series was smoothed 7 times, corresponding to a maximum smoothing $\sim$ 13 ms. If a pulse is detected in more than one of the smoothed time series, only the highest S/N result is recorded. Most pulses were optimally detected with smoothings of 2 or 3 samples, equivalent to widths of $\sim$ 64 or 128 μs. Pulses that are strongest at DM = 0 pc cm^{-3} are not included. UPPER LEFT: Histogram of S/N for identified pulses for S/N > 5 (solid line). Note the logarithmic scale of the y-axis. The dashed line shows the Gaussian distribution expected for noise only. UPPER MIDDLE: Number of pulses above a 5 σ threshold vs. DM channel. The lower x-axis shows DM channel number, while the upper x-axis shows DM in pc cm^{-3}. A broadened peak at the DM of the Crab is obvious. UPPER RIGHT: Scatter plot of DM and S/N. The largest values of S/N occur at or near the DM of the pulsar while the scatter of points uniform over DM and extending to S/N $\sim$ 14 is caused by strong RFI at $\sim$ 90 sec in the time series shown in the bottom frame. BOTTOM: All pulses with S/N greater than 5 σ plotted vs. DM channel and time. The size of the circle is linearly proportional to the S/N of the pulse, with the largest circle representing a S/N $\sim$ 23. As shown in Figures 3 and 4, strong pulses at high frequencies may be detected across many DM channels.

3.6. *Diagnostics*

Once all smoothed, dedispersed time series have been searched for pulses above threshold, the output must be examined to determine whether these pulses are of astrophysical origin. This can be done by creating diagnostic plots like those shown in Figures 5 and 6, which show example search output[5] for the giant-pulse emitting pulsars PSR B0531+21 and PSR B1937+21. While the examples here are from a search for single pulses from pulsars, the analysis method is applicable to searches for any transient radio signals.

The data for PSR B0531+21 were taken at the Arecibo Observatory at a frequency of 2330 MHz across a 100 MHz bandpass with the Wideband Arecibo Pulsar Processor (WAPP, `http://www.naic.edu/~wapp/`) with 64 frequency channels and 32 μs sampling. The data for PSR B1937+21 were taken at a frequency of 430 MHz across a 10-MHz bandpass with the Arecibo Observatory Fourier Transform Machine (AOFTM, `http://www.naic.edu/~aoftm/`), which has 1024 frequency channels and 102.4 μs sampling. While the WAPP uses 16-bit sampling, the AOFTM uses two-bit sampling, which will limit the measured dynamic range of giant pulses.

The data for both pulsars were dedispersed across a range of trial DMs using the post-detection method as described in §3.3. As discussed, DM channels are spaced more coarsely at higher DMs. A single-pulse search was carried out as described in §3.4. Figures 5 and 6 each show histograms of S/N and of DM, a scatter plot of S/N and DM, and a time series of events above a threshold (S/N > 5 and 4, respectively, for B0531+21 and B1937+21). In the absence of any signal (celestial or RFI), we expect the distribution of S/Ns to be Gaussian. For a time series with N samples and $N_{\rm DM}$ trial values of DM, the number of detections per bin of size Δ in S/N is

$$\Delta N_p \approx 2NN_{\rm DM}\Delta f(\text{S/N}), \qquad (18)$$

where f(S/N) is a Gaussian probability density function with unit variance. The dashed lines in the upper left panels of Figures 5-6 are plots of ΔN_p for the two cases.

The S/N histograms for both pulsars clearly deviate from a Gaussian distribution at high values of S/N. In the absence of signal, we also expect the DM distribution of pulses to be flat, in the mean, with fluctuations obeying Poisson statistics. The DM distributions clearly deviate from this form, showing well-defined peaks at the dispersion measures of the pulsars. From Eq. 17, the expected number of pulses above threshold due to

[5] Similar plots for a number of pulsars can be found at `http://www.jb.man.ac.uk/~mclaughl/single` and at `http://www.astro.cornell.edu/~cordes`.

radiometer noise alone ≈ 12 and 260 for the data in Figures 5 and 6, respectively. The baseline (i.e. in DM channels other than that of the pulsar) number of pulses above threshold for PSR B0531+21 is higher than this number because, as discussed in §3.3.3, strong, high-frequency pulses may be detected across a broad range of DM channels. The baseline number of pulses for the lower frequency observation of PSR B1937+21 is similar to that predicted for Gaussian noise, aside from a peak at zero DM due to RFI. The lower halves of Figures 5 and 6 show the strongest individual pulses plotted vs. DM and time, with the size of the circle proportional to S/N. This plot is complementary to the DM histogram; sources which emit many weak pulses may be detected in the DM

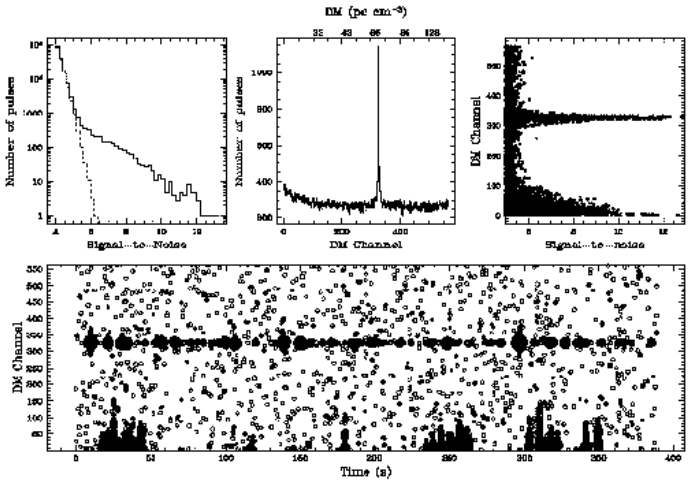

FIG. 6.— Single-pulse search results for PSR B1937+21 at 430 MHz shown in the same format as Figure 5 and using a threshold of 4 σ. This millisecond pulsar has DM = 71.04 pc cm^{-3} and period-averaged 430-MHz flux density ∼ 200 mJy. Most pulses were detected with no smoothing, equivalent to pulse widths $\lesssim$ 0.1 ms. The values of S/N are saturated because the data acquisition system provides only 2-bit output samples, 1024 of which are summed in the dedispersion procedure. The narrowness of the histogram of DM values for detected pulses (upper middle panel) is consistent with the narrow pulse widths and Eq. 14, as demonstrated in Figure 4. While there is RFI at low DMs, an excess of strong pulses at the DM of the pulsar is obvious.

4. INTERSTELLAR SCATTERING AND SCINTILLATION

In this section, we describe the basic scattering and scintillation phenomena that are relevant to the detection and identification of transient celestial signals. The two main effects are pulse broadening and intensity scintillations. Both affect the detectability of transient signals. Pulse broadening always decreases S/N while scintillation can increase or decrease S/N. In addition, these effects can signify whether a given candidate transient is truly celestial.

The degree of scattering is strongly frequency, direction, and distance dependent. Moreover, source sizes strongly influence the fractional intensity modulation of scintillation. Sources compact enough to emit fast transients will generally show scintillations at centimeter (and longer) wavelengths. In the following, we describe quantitative aspects of scattering and scintillation, observing regimes and optimal detection strategies.

4.1. *Basic Phenomena*

Multipath scattering of radiation from electron-density variations in the ISM produces the pulse-broadening effect discussed in §3.2. It also produces scintillations that modulate the measured intensity. Diffractive interstellar scintillations (DISS), which occur in the so-called strong scattering regime, produce intensity variations with characteristic frequency scales $\Delta\nu_{\rm d} \ll \nu$. DISS is caused by small-scale irregularities in the interstellar plasma and, for observations at meter wavelengths, has typical time and frequency scales of order minutes and MHz, with large variations that depend on DM, frequency and direction. Longer term, relatively broadband intensity variations of timescales of days to months are caused by refractive interstellar scintillations (RISS), associated with larger-scale irregularities than those responsible for DISS. In the strong scattering regime, DISS and RISS are distinct phenomena. The intensity modulation from DISS, $g_{\rm d}$, is a random variable with one-sided exponential statistics and 100% fractional variation for an intrinsically pointlike source. The modulation from RISS, $g_{\rm r}$, has a more symmetric distribution with smaller rms variation of a few tens of percent. Reviews of the phenomena may be found in Rickett (1990) and Narayan (1992). In weak scattering, DISS and RISS merge to produce fractional intensity variations of less than unity. The transition from strong to weak scattering depends strongly on direction. For lines of sight looking out of the Galactic plane, it is typically ∼ 5 GHz, but for the Galactic center the transition is higher than 100 GHz.

4.2. *Source Size Requirements and Coherence*

Sources must be compact for DISS and RISS to occur. In the strong scattering regime, a point source will be broadened to a size θ_d that is typically in the range of 1 mas to 1 arcsec at 1 GHz. The resultant diffraction pattern at an observer's location has spatial scale $\ell_d \sim \lambda/\theta_d$, where λ is the wavelength. By reciprocity, sources with spatial extents larger than $\sim \ell_d$ will diminish the fractional modulation of DISS (apart from 'leveraging' effects associated with the scattering region being closer to the source or to the observer, which we discuss below). We define the isoplanatic angular size as $\theta_{\rm iso} \propto \ell_d/D \propto \lambda/D\theta_d$, where D is the distance to the source and the proportionality constant depends on the location and depth of the scattering region along the line of sight. For RISS, the isoplanatic scale $\ell_r \sim D\theta_d$ and the isoplanatic angular size is $\theta_{\rm iso} \propto \theta_d$. At 1 GHz, and for path lengths through the ISM ∼ 1 kpc, the isoplanatic angular scale $\theta_{\rm iso} \sim 10^{-7}$ arc sec for DISS and $\sim 10^{-3}$ arc sec for RISS, though with large variations.

Transient sources producing short-duration signals are compact enough to satisfy these criteria in some cases. Given the light-travel size for a source at 1 kpc, signals shorter than 50 ms will show fully-modulated DISS while signals shorter than 500 s will show fully-modulated RISS. Relativistic motions, of course, will alter these estimates, by increasing the light-travel source size by a Doppler factor $D_\gamma = 1/\gamma(1-\beta\cos\theta) \approx 2\gamma$ for $\gamma \gg 1$ (where

γ is the Lorentz factor of bulk motion in the source). The transverse size is relevant for scintillation quenching, however, and is related to the light-travel size in a model-dependent way.

For longer path lengths or larger scattering strengths, the isoplanatic angle for DISS becomes smaller while that for RISS becomes larger. For an extragalactic source, the greater distance increases the allowed signal durations while, if viewed at Galactic latitudes $\gtrsim 10^\circ$ and for similar host galaxy inclinations, the scattering angular size (θ_d) remains small.

As is well known, fast transients necessarily arise from coherent emission if the measured transient signature is intrinsic and implies a brightness temperature in excess of physically plausible limits. Using the same light-travel size as before, the brightness temperature is

$$T_b \approx 10^{14.8}\, K\, S_{\rm mJy} \left(\frac{D_{\rm kpc}}{\nu_{\rm GHz}\Delta t}\right)^2; \qquad (19)$$

$S_{\rm mJy}$ is the flux density in mJy and Δt is the signal duration. Relativistic motion decreases the coefficient by a factor $\sim 1/4\gamma^2$ for $\gamma \gg 1$. Sources compact enough to show DISS (i.e. $\Delta t \lesssim 50$ ms for $\gamma \sim 1$) have $T_b \gtrsim 10^{17.4}\, K$ for other parameters held fixed in Eq. 19. This is too large to be associated with incoherent processes.

4.3. *Expected Timescales and Bandwidths*

Both DISS and pulse broadening are well established for Galactic pulsars. RISS has been identified in observations of AGNs and masers as well as pulsars. For a given combination of line of sight and frequency, DISS and pulse broadening are typically mutually exclusive in pulsars, because when the pulse broadening is large enough to be identified, the scintillation bandwidth is too small to be measured, as indicated by values plotted in Figure 2. Exceptions occur, of course, because the identification of pulse broadening is a function of intrinsic pulse width.

Quantitatively, the pulse broadening time τ_d and the scintillation bandwidth $\Delta\nu_{\rm d}$ are reciprocally related by $2\pi\tau_d\Delta\nu_{\rm d} = C_1$ (e.g. Cordes & Rickett 1998). For a uniform medium with Kolmogorov fluctuations, $C_1 = 1.16$. Otherwise, $C_1 \sim 1$, except for scattering in thin screens near the source or observer. For typical pulsar pulses, pulse broadening is manifest when $\tau_d \gtrsim 1$ ms, in which case the scintillation bandwidth is too small to be resolved (for typical source flux densities and spectrometer resolutions). Exceptions to this are the Crab pulsar's giant pulses, which show structure in the range of a few nanoseconds to a few microseconds (Hankins 2003). These narrow pulses allow measurement of much smaller pulse broadening times, corresponding to measurable scintillation bandwidths. If other sources of very narrow pulses exist (e.g. $W \ll 1$ ms), then scintillation frequency structure will be measureable for them as well.

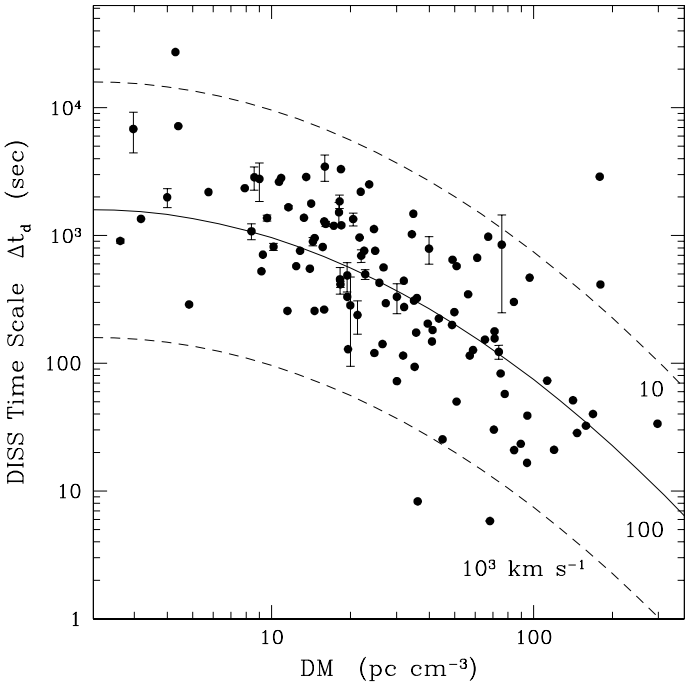

FIG. 7.— The characteristic DISS timescale at 1 GHz plotted against DM for a sample of pulsars. For objects with multiple observations, the vertical bars designate the $\pm 1\sigma$ variation of the mean value. The solid and dashed lines show predicted DISS timescales for transverse source velocities of 10, 100 and 10^3 km s^{-1} using Eqs. 6 and 21 and the relation $2\pi\tau_d\Delta\nu_{\rm d} = C_1$ (see text). For these curves, we also assume the scattering medium is statisically uniform, which is approximate at best, and we do not include the scatter in values about Eq. 6 evident in Fig 2. The DISS timescale varies with frequency as $\Delta t_{\rm d} \propto \nu^{1.2}$ if the scintillation bandwidth has the Kolmogorov scaling, $\Delta\nu_{\rm d} \propto \nu^{4.4}$, as appears consistent for some objects. For extragalactic sources, the DISS time scale will differ because the geometry of the scattering medium consists of a foreground region from the Galaxy and another region corresponding to material in the host galaxy (if any). Nonetheless, the order of magnitiude value of the time scale can be estimated using the value of DM expected from just the foreground material in the Galaxy (see Appendix A). The points are from Bhat et al. (1999); Bogdanov et al. (2002); Camilo & Nice (1995); Cordes (1986); Dewey et al. (1988); Foster et al. (1991); Fruchter et al. (1988); Gothoskar & Gupta (2000); Johnston et al. (1998); NiCastro et al. (2001); and Phillips & Clegg (1992).

While the pulse broadening timescale and DISS bandwidth depend on the distribution of scattering material along the line of sight, the DISS timescale $\Delta t_{\rm d}$ also depends on the source's velocity. The scintillation velocity, $V_{\rm ISS}$, is the speed of the ISS diffraction pattern across the LOS and determines the scintillation timescale as

$$\Delta t_{\rm d} \equiv \frac{\ell_d}{V_{\rm ISS}} = W_1 \frac{\ell_d}{V_{\rm s\perp}} = \frac{W_2}{\nu V_{\rm s\perp}} \left(\frac{cD\Delta\nu_{\rm d}}{4\pi C_1}\right)^{1/2}, \qquad (20)$$

where $V_{\rm s\perp}$ is the source velocity and $W_{1,2}$ are weighting factors that take into account the location of scattering material along the LOS (c.f. Cordes & Rickett 1998, Eq. 4, 9, 17 and 23). The final equality in Eq. 20 follows by relating the spatial scale ℓ_d to the scintillation bandwidth $\Delta\nu_{\rm d}$ and other quantities by using $\ell_d = \lambda/\theta_d$ (c.f. §4.2) along with the proportionality $\tau_d \propto D\theta_d^2/2c$ and the equation relating τ_d to $\Delta\nu_{\rm d}$. For nominal values, and assuming a Kolmogorov spectrum for the scattering irregularities, the scintillation timescale is

$$\Delta t_{\rm d} = 252\, s\, W_2 (cD_{\rm kpc}\Delta\nu_{\rm d,MHz})^{1/2} (\nu_{\rm GHz} V_{\rm s\perp,100})^{-1}, \qquad (21)$$

where $V_{s\perp,100} = V_{s\perp}/(100\,\mathrm{km\,s^{-1}})$ and $W_2 = 1$ for a uniform medium. Pulsars have 3D velocities that average $\sim$ 400 km s^{-1} (e.g. Cordes & Chernoff 1998), so their scintillation timescales can be quite short. Other Galactic sources may be slower and would accordingly have longer scintillation timescales. Note that since $\Delta\nu_\mathrm{d} \propto \nu^{4.4}$ for a Kolmogorov wavenumber spectrum for the electron-density irregularities, $\Delta t_\mathrm{d} \propto \nu^{1.2}$ in the strong-scattering regime. In weak scattering the characteristic scintillation bandwidth $\approx \nu$ and the level of modulation becomes less. Figure 7 shows the scintillation time scale for known pulsars along with estimates based on Eq. 21 for transverse velocities of 10, 100 and 10^3 km s^{-1}.

4.4. *Comparison of Galactic and Extragalactic Source Scintillations*

In some circumstances, the scintillations of fast radio transient sources can serve as a 'reality check' on the astrophysical nature of the emission, based on the direction, distance and frequency of observation. In order to estimate the DISS and pulse broadening properties of extragalactic transient sources, we have developed the formalism in the Appendix. As shown there, we expect scintillation timescales for extragalactic sources to be about one-third as much as for Galactic sources in the same direction. We also find that the pulse broadening time for an extragalactic source will be approximately six times larger than for a Galactic source in the same direction. Similarly, scintillation bandwidths for extragalactic sources will be about six times smaller.

4.5. *Optimal Observing Strategy in the Strong Scattering Regime*

DISS in the strong scattering regime can both help and hinder detection of transient radio signals. Signals too weak to be detected without the scattering medium may be modulated above the detection threshold while stronger signals that are nominally above the threshold can be modulated below. As shown in Cordes & Lazio (1991), in the strong scattering regime (i.e. distances $\geq$ 1 kpc at $\sim$ 1 GHz), multiple observations of a given target comprise a strategy that can be superior to single observations even when the total time per target is held fixed. The requirements for favoring this strategy are that (a) the source size is much smaller than the isoplanatic size and (b) that there is no bandwidth averaging of the DISS frequency structure.

We now define several observational regimes. In radio transient searches, it is useful to consider the dynamic spectrum (intensity as a function of time and frequency) as the analyzable data unit. We follow Cordes & Lazio (1991), who define the number of independent scintillation fluctuations ('scintles') contained in a frequency-time resolution element of size $\Delta\nu \times \Delta t$ as

$$N_\mathrm{ISS} = N_t N_\nu, \tag{22}$$

$$N_t \approx 1 + \eta\Delta t/\Delta t_\mathrm{d}, \tag{23}$$

$$N_\nu \approx 1 + \eta\Delta\nu/\Delta\nu_\mathrm{d}, \tag{24}$$

where $\eta \approx 0.1 - 0.2$ is a 'filling' constant. Given the large variation in scintillation parameters (c.f. Figure 2 and Eq. 21), N_ISS varies by orders of magnitude as a function of frequency and DM. For fast transients, we expect $\Delta t \ll \Delta t_\mathrm{d}$, so that $N_t = 1$. However, if differential dispersive arrival times span a long time, which will be true for large DM or low frequencies, the dedispersed signal may span one or more independent 'scintles' and $N_t > 1$. For broadband transients, optimal detection requires integration over frequency (with implied dedispersion), in which case it may also be true that $N_\nu \gg 1$. Narrowband transients, such as may be expected from masers and from signals from extraterrestrial intelligence, are likely to have $N_\nu = 1$, except for long lines of sight through the inner Galaxy combined with observations at low frequencies, for which $\Delta\nu_\mathrm{d}$ can be less than 1 Hz.

Three scintillation regimes may be identified in terms of N_ISS. We assume that the strong scattering regime applies and that the source size is much smaller than the isoplanatic angular size:

1. $N_\mathrm{ISS} = 1$: The measured signal will be 100% modulated and the intensities will be exponentially distributed.

2. $1 \lesssim N_\mathrm{ISS} \lesssim 100$: The scintillations will be less than 100% modulated and will have a χ^2 distribution with $\sim 2N_\mathrm{ISS}$ degrees of freedom. For $N_\mathrm{ISS} \gtrsim 5$, the distribution is well described as a Gaussian function. Fast transients with $N_t = 1$ in this regime have multiple scintles across the frequency range $\Delta\nu$. Each scintle has an amplitude described by the exponential distribution. Before integrating over frequency, the optimal S/N may result by weighting the individual amplitudes to favor the strong scintles.

3. $N_\mathrm{ISS} \gg 100$: The DISS modulation of the combined signal (after integrating over time and frequency) $\lesssim 10\%$.

In the first regime, where the signal is fully modulated, an optimization strategy that maximizes the detectability of a source with respect to DISS comprises multiple observations. In a single observation, it is more likely that the signal is modulated below its mean (probability $= 1 - e^{-1}$) than above it. Less frequently, a large boost in signal strength is expected because the modulation has an exponential distribution. If the total amount of telescope time is fixed and divided into N subobservations separated by more than a characteristic scintillation time, there is an optimal, finite value of N. For an *intrinsically steady* source, the optimal number of trials ~ 3 maximizes the probability that *at least* one detection is made. For transient sources, the optimization also depends on the (unknown) intrinsic distribution of emitted amplitudes. For infrequent or single-instance transients, DISS in the first regime will on average degrade the detectability of a given source. However, across a population of sources the DISS will aid detection in $\sim e^{-1}$ of the cases and hinder detection in the remainder.

5. RADIO FREQUENCY INTERFERENCE

Radio frequency interference is a growing problem for radio astronomy in general and for the detection of transient signals in particular. Considerable work is now

being done on identifying and mitigating RFI in a number of ways. A situation similar to pulse detection in the time domain is the detection of narrow spectral lines. As discussed by Horowitz & Sagan (1993), RFI from artificial, terrestrial sources can be identified, in part, by requiring candidate signals to conform to what is expected from celestial signals. For narrow spectral lines, one expects variable Doppler shifts in accordance with Earth's spin and orbital motion. As shown by Horowitz & Sagan, however, even this requirement allows rare RFI to satisfy basic requirements that a real, celestial signal must satisfy. For time domain searches, such as those we have focused on here, RFI can mimic the dispersive arrival times of pulses in instances where the RFI is a swept-frequency signal. Thus, while filters based on anticipated properties of celestial signals are necessary elements of transient searches, they are not sufficient for providing candidate detections that are devoid of false positive detecions.

To identify real celestial transients while rejecting RFI, searches using single pixel systems must rely on application of tests for properties that real, celestial signals must have, including Doppler shifts and dispersive arrival times, and also any repeatability of the transients that can be explored through multiple observations and on-and-off source comparisons. Scintillations play an important role in tests for repeatability, especially for compact sources that underly fast transients, as discussed in Cordes, Lazio & Sagan (1997).

6. CONCLUSIONS

We have described issues related to and methods for searching for fast radio transients. A very small parameter space of the transient radio sky has been explored thus far. While we have gained an excellent understanding of the high-energy transient sky through X-ray and gamma ray satellites, radio searches for transient sources have been limited by the small sky coverage and high susceptibility to RFI of current telescopes. To increase the capabilities of single-pulse searches, systems with multiple beams or multiple antennas are necessary in order to perform coincidence tests which will discriminate between pulses of astrophysical and terrestrial origins. Radio telescopes with larger fields of view are necessary to maximize the chances of detecting radio-bursting objects and to complement the searches at high-energies. Larger collecting areas are needed to increase our sensitivity to pulses from pulsars and other transient sources in other galaxies. Multi-beam systems for the Arecibo and Green Bank telescopes will likely be built within the next few years. Observing with multiple beams will allow us to distinguish RFI from real signals. On a longer time scale, large radio arrays such as the Square Kilometer Array (SKA) will be developed. With a planned field of view over 100 times that of Arecibo and a sensitivity over 20 times that of Arecibo, the SKA will revolutionize our understanding of the transient radio sky. While the SKA will not be operational for many years, single-pulse searches in the meantime, especially with multiple beams, are essential for optimizing routines for RFI excision and for processing large amounts of data. With more sensitive instruments and more sophisticated analyses, the next few decades will undoubtedly bring about a greater understanding of radio-bursting objects, including Crab-like pulsars in other galaxies, counterparts to high-energy bursting sources, and other classes of objects which are yet to be discovered.

We thank Joe Lazio and Ira Wasserman for useful discussions. This work was supported by NSF grants AST9819931, AST0138263 and AST0206036 to Cornell University. MAM is also supported by an NSF Math and Physical Sciences Distinguished Research Fellowship. Arecibo Observatory is operated by the National Astronomy and Ionosphere Center, which is operated by Cornell University under cooperative agreement with the National Science Foundation (NSF). The Parkes Observatory is part of the Australia Telescope which is funded by the Commonwealth of Australia for operation as a National Facility managed by CSIRO.

REFERENCES

Aller, H. D., Aller, M. F., Latimer, G. E., & Hodge, P. E. 1985, ApJS, 59, 513
Amy, S. W., Large, M. I., & Vaughan, A. E. 1989, Proceedings of the Astronomical Society of Australia, 8, 172
Aubier, A., Boudjada, M. Y., Moreau, P., Galopeau, P. H. M., Lecacheux, A., & Rucker, H. O. 2000, A&A, 354, 1101
Backer, D. C., Dexter, M. R., Zepka, A., Ng, D., Werthimer, D. J., Ray, P. S., & Foster, R. S. 1997, PASP, 109, 61
Berger, E. et al. 2001, Nature, 410, 338
Bhat, N. D. R., Rao, A. P., & Gupta, Y. 1999, ApJS, 121, 483
Bogdanov, S., Pruszyńska, M., Lewandowski, W., & Wolszczan, A. 2002, ApJ, 581, 495
Camilo, F. & Nice, D. J. 1995, ApJ, 445, 756
Cognard, I., Shrauner, J. A., Taylor, J. H., & Thorsett, S. E. 1996, ApJ, 457, L81
Cohen, R. J. & Brebner, G. C. 1985, MNRAS, 216, 51P
Colgate, S. A. & Noerdlinger, P. D. 1971, ApJ, 165, 509
Cordes, J. M. 1986, ApJ, 311, 183
Cordes, J. M. & Lazio, T. J. 1991, ApJ, 376, 123
Cordes, J. M., Lazio, T. J. W., & Sagan, C. 1997, ApJ, 487, 782
Cordes, J. M. & Chernoff, D. F. 1998, ApJ, 505, 315
Cordes, J. M. & Lazio, T. J. W. L. 2002, astro-ph/0207156
Cortiglioni, S., Mandolesi, N., Morigi, G., Ciapi, A., Inzani, P., & Sironi, G. 1981, Ap&SS, 75, 153
Davies, J. G., & Large, M. I., 1970, MNRAS, 149, 301
Dewey, R. J., Cordes, J. M., Wolszczan, A., & Weisberg, J. M. 1988, AIP Conf. Proc. 174: Radio Wave Scattering in the Interstellar Medium, 217
Edwards, P. J., Hurst, R. B., & McQueen, M. P. C., 1974, Nature, 247, 444
Foster, R. S., Fairhead, L., & Backer, D. C. 1991, ApJ, 378, 687
Fruchter, A. S., Taylor, J. H., Backer, D. C., Clifton, T. R., & Foster, R. S. 1988, Nature, 331, 53
Goodman, J. 1997, New Astronomy, 2, 449
Gothoskar, P. & Gupta, Y. 2000, ApJ, 531, 345
Hansen, B. M. S. & Lyutikov, M. 2001, MNRAS, 322, 695
Hankins, T. H. 1971, ApJ, 169, 487
Hankins, T. H. & Rickett, B. J. 1975, Methods in Computational Physics. Volume 14 - Radio astronomy, 14, 55
Hankins, T. H. et al. 1981, ApJ, 244, L61
Hankins, T. H. et al. 2003, Nature, 422, 141.
Harris, D. E., Zeissig, G. A., & Lovelace, R. V. 1970, A&A, 8, 98
Hesse, K. H. & Wielebinski, R. 1974, A&A, 31, 409
Hewish, A., Bell-Burnell, J., Pilkington, J. D. H., Scott, P. F., & Collins, R. A, 1968, it Nature, 217, 709
Horowitz, P. & Sagan, C. 1993, ApJ, 415, 218
Hughes, V. A. & Retallack, D. S., 1973, *Nature*, 242, 105
Huguenin, G. R. & Moore, E. L. 1974, ApJ, 187, L57
Inzani, P., Sironi, G., Mandolesi, N., & Morigi, G. 1982, AIP Conf. Proc. 77: Gamma Ray Transients and Related Astrophysical Phenomena, 79
Jackson, P. D., Kundu, M. R., & White, S. M. 1989, A&A, 210, 284
Johnston, S., Nicastro, L., & Koribalski, B. 1998, MNRAS, 297, 108
Johnston, S. & Romani, R. W. 2003, ApJ, submitted.
Kardashev, N. S. et al. 1977, Soviet Astronomy, 21, 1
Kedziora-Chudczer, L. L., Jauncey, D. L., Wieringa, M. H., Tzioumis, A. K., & Reynolds, J. E. 2001, MNRAS, 325, 1411
Lainela, M. 1994, A&A, 286, 408
Lambert, H. C. & Rickett, B. J. 1999, ApJ, 517, 299.
Lecacheux, A., Boudjada, M. Y., Rucker, H. O., Bougeret, J. L., Manning, R., & Kaiser, M. L. 1998, A&A, 329, 776
Linscott, I. R. & Erkes, J. W. 1980, ApJ, 236, L109
Löhmer, O., Kramer, M., Mitra, D., Lorimer, D. R., & Lyne, A. G. 2001, ApJ, 562, L157.
Mann, G., Klassen, A., Classen, H.-T., Aurass, H., Scholz, D., MacDowall, R. J., & Stone, R. G. 1996, A&AS, 119, 489
McCulloch, P. M., Ellis, G. R. A., Gowland, G. A., & Roberts, J. A. 1981, ApJ, 245, L99
Narayan, R. 1992, Phil. Trans. R. Soc. Lond. A, 341, 151.
Nicastro, L., Nigro, F., D'Amico, N., Lumiella, V., & Johnston, S. 2001, A&A, 368, 1055
Nice, D. J., Fruchter, A. S., & Taylor, J. H. 1995, ApJ, 449, 156
Nice, D. J. 1999, ApJ, 513, 927
O'Sullivan, J. D., Ekers, R. D., & Shaver, P. A. 1978, Nature, 276, 590
Phillips, J. A. & Clegg, A. W. 1992, Nature, 360, 137
Phinney, S. & Taylor, J. H. 1979, Nature, 277, 117
Poquerusse, M., Steinberg, J. L., Caroubalos, C., Dulk, G. A., & MacQueen, R. M. 1988, A&A, 192, 323
Rees, M. J. 1977, Nature, 266, 333
Rickett, B. J., 1990, ARA&A, 28, 561
Romani, R. W. & Johnston, S. 2001, ApJ, 557, L93.
Staelin, D. H. & Reifenstein, E. C., 1968, *Science*, 162, 1481
Taylor, J. H., Huguenin, G. R., & Hirsch, R. M. 1972, ApJ, 172, L17
Taylor, J. H., Backus, P. R., & Damashek, M. 1981, ApJ, 244, L65
Taylor, J. H., Manchester, R. N., & Lyne, A. G., 1993, ApJS, 88, 529
Turtle, A. J., Campbell-Wilson, D., Bunton, J. D., Jauncey, D. L., & Kesteven, M. J. 1987, Nature, 327, 38
Weber, J. 1969, *Phys. Rev. Letters*, 22, 1320
Williamson, I. P. 1972, MNRAS, 157, 55.
Yudaeva, N. A. 1986, Soviet Astronomy Letters, 12, 150

APPENDIX

INTERSTELLAR SCATTERING AND SCINTILLATION OF SOURCES IN OTHER GALAXIES

Scattering of radio waves from electron-density variations produces angular blurring (or 'seeing') of radio sources and (for variable sources) temporal broadening due to multipath propagation. Under certain conditions, radiation from a source of spatially coherent emission will show scintillation from interference between the differentially-arriving wavefronts and from refractive changes in the radius of curvature of the wavefronts. These various effects are associated with different line-of-sight (LOS) weightings of the scattering material. Here we take these weightings into account when deriving estimates for scattering and scintillations of extragalactic sources.

The phase structure function may be used to calculate the angular scattering and scintillation timescale. This function, as given by Cordes & Rickett (1998; Eq. 2), is

$$D_\phi(\boldsymbol{\delta x}, \delta t) = (\lambda r_e)^2 f_\alpha \int_0^D ds\, C_n^2(s) \left| \mathbf{V}_{\rm eff,\perp}\delta t + \left(\frac{s}{D}\right)\boldsymbol{\delta x}_\perp \right|^\alpha , \tag{A1}$$

assuming that diffraction involves only small angles and that the underlying structure function for the electron density is isotropic and scales as $|\boldsymbol{\delta x}|^\alpha$, where $\alpha + 2$ is the power law index of the electron density wavenumber spectrum. For a Kolmogorov wavenumber spectrum, $\alpha = 5/3$, subject to constraints on the wavenumber cutoffs. In Eq. A1, λ is the wavelength, r_e is the classical electron radius, f_α is a constant of order unity which depends on α, $\mathbf{V}_{\rm eff}$ is the effective velocity of the source, and D is the distance to the source. The integral is calculated from $s = 0$ at the source to $s = D$ at the observer's location and $\mathbf{V}_{\rm eff}$ is

$$\mathbf{V}_{\rm eff}(s) = \left(1 - \frac{s}{D}\right)\mathbf{V}_{\rm s} + \left(\frac{s}{D}\right)\mathbf{V}_{\rm obs} - \mathbf{V}_{\rm m}(s), \tag{A2}$$

where $\mathbf{V}_{\rm s}$, $\mathbf{V}_{\rm obs}$ and $\mathbf{V}_{\rm m}$ are the velocities of the source, observer and medium (all relative to a common standard of rest). Only the components perpendicular to the LOS affect the time scales of diffractive interstellar scintillation (DISS).

In the following we assume that the scattering is 'strong,' in the sense that the phase perturbation induced by scattering irregularities is larger than one radian when one considers two ray paths separated by a Fresnel scale. For a single thin screen, this scale is well defined, whereas for a distributed scattering medium one must weight the scattering material according to a factor determined by where it lies along the path. For further details, see Rickett (1990).

Angular Broadening

First we consider angular broadening (i.e. "interstellar seeing"). The observed angular diameter of a source is related inversely to the transverse scale on which $D_\phi(\boldsymbol{\delta x}, 0) = 2$. The integral for D_ϕ weights scattering material by $(s/D)^{5/3}$ (for a Kolmogorov spectrum) and thus favors material nearest the observer. For objects in other galaxies, we therefore ignore contributions to D_ϕ from the host galaxy. Consider an extragalactic source at distance D and Galactic latitude b and a Galactic source at the same latitude but at distance $D_{\rm g}$. Introducing the scattering measure, defined as $\mathrm{SM} = \int_0^D ds\, C_n^2(s)$, the ratio of angular diameters of these sources as seen by an observer in the Milky Way is

$$\frac{\theta_{\rm FWHM}({\rm xgal})}{\theta_{\rm FWHM}({\rm Gal})} = \left(\frac{\mathrm{SM_{Gal}}}{\int_0^{\rm D_g} ds\, C_n^2(s)(1 - s/D_{\rm s})^\alpha}\right)^{1/\alpha} \geq 1, \tag{A3}$$

where $\mathrm{SM_{Gal}}$ is the Galactic contribution to SM in the direction to the source. The integral in the denominator is over the line of sight to the source, with the integration now going from observer (at $s = 0$) to source. Assuming an exponential distribution for C_n^2 and considering a Galactic source at distance $D_{\rm g}$ equal to one exponential scale height H, we find $\theta_{\rm FWHM}({\rm xgal})/\theta_{\rm FWHM}({\rm Gal}) \approx 2.1$. This approximate doubling of the angular diameter of an extragalactic source viewed through the same medium as a Galactic source results from the much smaller curvature of the extragalactic source's wavefronts impinging on the ISM and can serve as a potential distance estimator for high-latitude transient sources.

Pulse Broadening

As discussed in Cordes & Lazio (2002), the pulse broadening timescale is proportional to $\mathrm{SM}_\tau^{6/5} D$, where

$$\mathrm{SM}_\tau = 6 \int_0^D ds\, (s/D)(1 - s/D) C_n^2(s). \tag{A4}$$

In contrast to angular broadening, the LOS weighting function is symmetric about the LOS midpoint, so a significant contribution is expected from the host galaxy as well as trom the Milky Way. Consider a pulsed source in the host galaxy and a path length through the host galaxy $D_{\rm xgal}$ and a path length through the Milky Way of $D_{\rm g}$. Both $D_{\rm xgal}$ and $D_{\rm g}$ are much less than the total distance, D. For simplicity, we assume that the scattering media in the two galaxies are uniform and that the intergalactic medium makes no contribution to the scattering. The ratio of the pulse-broadening time for the extragalactic object to that for a Galactic source at distance $D_{\rm g}$ from the observer is

$$\frac{\tau_{d\rm xgal}}{\tau_{d\rm Gal}} \approx 3.7 \left(1 + \frac{\mathrm{SM_{xgal}} D_{\rm xgal}}{\mathrm{SM_{Gal}} D_{\rm g}}\right)^{6/5} \left(\frac{D_{\rm g}}{D}\right)^{1/5} . \tag{A5}$$

The particular form (with the exponent of 6/5 and the ratio of distances to the 1/5 power) follows from the assumption that scattering is dominated by the power law portion of the wavenumber spectrum and not the inner scale of the spectrum. For intense scattering at low frequencies, the inner scale may play a role, in which case $6/5 \to 1$ and the ratio of distances is replaced by unity (see Cordes & Lazio 2002 for details). The factor of 3.7 in Eq. A5 results from the fact that the Galaxy's ISM sees spherical waves from Galactic sources but plane waves from extragalactic sources. Similarly, the host galaxy's ISM sees spherical waves from the emitting source. When the second term in square brackets is unity (equal contributions from the host galaxy and the Milky Way), the coefficient of the factor $(D_{\rm g}/D)^{1/5}$ becomes 8.5. For a pulsar in the Large Magellanic Cloud ($D \approx 50$ kpc), for example, the net ratio is about 3.9 for $D_{\rm g} = 1$ kpc. For an object in M33 ($D \approx 900$ kpc), the ratio is about 2.2. Accordingly, the scintillation bandwidths are a factor of two to four smaller. Of course, scattering in the host galaxy could be much larger than the Galactic scattering, yielding much larger τ_d and much smaller $\Delta\nu_d$. Representative values of $\tau_{d\rm Gal}$ can be read off of Figure 2 by approximating DM $\approx 30/\sin|b|$ pc cm^{-3}.

Scintillation Time Scale

We calculate $\Delta t_{\rm d}$, the scintillation timescale for DISS, using $D_\phi(0, \delta t) = 1$ to define the $1/e$ scale of the intensity correlation function. The LOS weightings in Eq. A1-A2 imply that contributions from both the host Galaxy and the Milky Way are important. With $s/D \ll 1$ for the host Galaxy, $\mathbf{V}_{\rm eff}(s) \approx \mathbf{V}_{\rm s} - \mathbf{V}_{\rm m}(s)$. For the portion of the LOS within the Milky Way, $s/D \to 1$ and $\mathbf{V}_{\rm eff}(s) = \mathbf{V}_{\rm obs} - \mathbf{V}_{\rm m}(s)$. Evaluating D_ϕ using the separate contributions to SM from the host galaxy ($\rm SM_{xgal}$) and the Milky Way ($\rm SM_{Gal}$), we find that

$$\Delta t_{\rm d} = \left[(\lambda r_e)^2 f_\alpha \left({\rm SM_{xgal}}|\mathbf{V}_{\rm s\perp} - \mathbf{V}_{\rm m\perp,xgal}|^\alpha + {\rm SM_{Gal}}|\mathbf{V}_{\rm obs\perp} - \mathbf{V}_{\rm m\perp,Gal}|^\alpha\right)\right]^{-1/\alpha} \tag{A6}$$

Eq. A6 implies that if the Galactic and extragalactic contributions to the SM are similar, both ends of the LOS contribute equally to $\Delta t_{\rm d}$. However if the source velocity exceeds the velocities of the observer and the interstellar media, as is typically the case with pulsars, then the contribution from the host galaxy will dominate the scintillation timescale. For this case, we calculate the ratio of $\Delta t_{\rm d}$ for an extragalactic source to that for a Galactic source as

$$\frac{\Delta t_{\rm d}({\rm xgal})}{\Delta t_{\rm d}({\rm Gal})} \approx \frac{|\mathbf{V}_{\rm s\perp}({\rm Gal})|}{|\mathbf{V}_{\rm s\perp}({\rm xgal})|}\left[\frac{\rm SM_{Gal}}{\rm SM_{xgal}}\int_0^1 dx\, e^{-x}x^\alpha\right]^{1/\alpha} \approx 0.36\frac{|\mathbf{V}_{\rm s\perp}({\rm Gal})|}{|\mathbf{V}_{\rm s\perp}({\rm xgal})|}\left[\frac{\rm SM_{Gal}}{\rm SM_{xgal}}\right]^{1/\alpha}, \tag{A7}$$

again assuming an exponential distribution for C_n^2 with a galactic source at a distance of one exponential scale height. Thus, along the same direction, we expect the scintillation timescale of an extragalactic source to be about 1/3 that of a Galactic source at a distance of one scale height for C_n^2. This result is more general than the analysis of Cordes & Rickett (1998), who considered the scintillation time for extragalactic sources under the assumption that the transverse velocity of the extragalactic source was negligible and that there was no contribution to SM from the host galaxy.

Weak Scintillation

When scattering is weak, the scintillations of a point source have a modulation index satisfying $\sigma_I/\langle I\rangle << 1$, the scintillations are correlated over a frequency range comparable to the (center) radio frequency, and any pulse broadening becomes smaller than the reciprocal radio frequency. The apparent source structure includes, in this regime, an unscattered component along with a scattered component. If $\sigma_\phi \ll 1$ is the rms phase variation between two paths separated by a Fresnel scale, $\sim (\lambda D/2\pi)^{1/2}$, then the fraction of the flux density in the scattered component $\sim \sigma_\phi^2$.

The transition frequency between weak and strong scattering may be evaluated (for Galactic sources) in terms of the scattering measure, SM, using an expression in Cordes & Lazio (2002),

$$\nu_{\rm trans} = 225\,{\rm GHz}\,{\rm SM}^{6/17}D_{\rm eff}^{5/17}, \tag{A8}$$

where $D_{\rm eff}$ is the effective distance to the scattering medium. For pulsars near the solar system with $\log {\rm SM} \approx -4$ and $D \approx 0.1$ kpc, $\nu_{\rm trans} \approx 4.4$ GHz. In the transition regime, scintillations behave similar to those in the strong scattering regime.